American Journal of Chemical Engineering
2026, Vol. 14, No. 3, pp. 60–75
https://doi.org/10.11648/j.ajche.20261403.12

Research Article

Kinetic and Thermodynamic Modelling of Zinc Adsorption Onto Acid-activated Oyster and Periwinkle Shells

Uzono Romokere Isotuk[1, *], Ukpong Anwana Abel[1], Ifiok Mfon Ibanga[2], Akwayo Iniobong Job[1], Sylvester Andrew Ekong[3]

[1]Department of Chemical/Petrochemical Engineering, Akwa Ibom State University, Uyo, Nigeria

[2]Department of Geology, Akwa Ibom State University, Uyo, Nigeria

[3]Department of Physics, Akwa Ibom State University, Uyo, Nigeria

Abstract

This study investigated the adsorptive removal of zinc ions (Zn^{2+}) from aqueous solution using low-cost biosorbents derived from periwinkle shell char (PSC, Tympanotonus fuscatus) and oyster shell char (OSC, Crassostrea gigas), activated with 1.0 M HCl following calcination at 600 ℃. Characterization by XRF and FTIR confirmed that both adsorbents are predominantly composed of calcite ($CaCO_3$), with calcium contents of 87.43% (PSC) and 91.26% (OSC), and exhibited surface hydroxyl and carbonate functional groups responsible for Zn^{2+} binding. Physicochemical analysis revealed specific surface areas of 186.4 m^2/g (PSC) and 214.7 m^2/g (OSC). Batch adsorption experiments were conducted to evaluate the effects of contact time, adsorbent dosage, temperature, initial Zn^{2+} concentration, and solution pH. Maximum Zn^{2+} removal of 82.6% (PSC) and 85.3% (OSC) was achieved at optimum conditions of pH 6.0, contact time of 60 min, adsorbent dosage of 1.0 g/100 mL, and temperature of 60 ℃. Adsorption kinetics were best described by the pseudo-first order model (R^2 = 0.927 for PSC; R^2 = 0.951 for OSC), with intraparticle diffusion identified as a contributing mechanism. Both Langmuir and Freundlich isotherm models satisfactorily correlated the equilibrium data; the Langmuir model yielded maximum monolayer adsorption capacities (qm) of 32.26 mg/g and 37.88 mg/g for PSC and OSC, respectively. Thermodynamic analysis revealed negative ΔG°, positive ΔH°, and positive ΔS° values, confirming that the adsorption process is spontaneous, endothermic, and associated with increased surface randomness. OSC consistently outperformed PSC across all parameters, attributable to its higher surface area, calcium content, and pore volume. These results demonstrate that both periwinkle and oyster shell chars are effective, sustainable, and low-cost adsorbents for zinc ion removal from wastewater.

Keywords

Zinc Adsorption, Periwinkle Shell Char, Oyster Shell Char, Langmuir Isotherm, Pseudo-first Order Kinetics, Wastewater Treatment, Bio Sorbent

*Correspondence: Uzono Romokere Isotuk (romokereuzono@aksu.edu.ng)

Received: 29 June 2026; **Accepted:** 8 July 2026; **Published:** 24 July 2026

1. Introduction

Water is an indispensable resource for sustaining life, constituting over 70% of the human body and serving as a critical medium for metabolic processes [1]. Therefore, having access to clean drinking water is a basic human right, and the World Health Organization (WHO) has established comprehensive guidelines governing potable water quality. The Nigerian Standard for Drinking Water Quality (NSDWQ), provides the legal foundation for regulating water safety nationwide in Nigeria. [2].

Despite these provisions, water quality in the Niger Delta region has experienced severe deterioration driven by rapid population growth, industrialization, and decades of oil and gas exploration. Many treatment facilities, constructed in the 1960s-1970s, are grossly inadequate in capacity and technology, while rural and semi-urban communities closest to industrial activity remain entirely reliant on untreated surface water [3].

Eastern Obolo Local Government Area, Akwa Ibom State, presents a particularly acute illustration of this crisis. As an oil-rich coastal community of twenty-eight villages lacking adequate water treatment infrastructure, the population depends on surface water from rivers and streams for domestic use [4]. Borehole installations have consistently degraded in quality, yielding turbid, saline water unfit for consumption. Of particular concern is heavy metal contamination, especially zinc, which enters aquatic environments through industrial discharge and oil field activities [4]. Prolonged exposure to elevated zinc concentrations has been associated with gastrointestinal distress, neurological impairment, and interference with essential trace element absorption, underscoring the need for effective and affordable remediation strategies.

Among heavy metal removal techniques, adsorption has consistently emerged as one of the most effective, simple, and cost-efficient approaches, particularly when low-cost adsorbents derived from locally available waste materials are utilized [5]. In this regard, oyster and periwinkle shells represent a highly promising class of bio-waste adsorbents, abundantly generated in the coastal communities of the Niger Delta where shellfish form a significant part of local dietary culture. Their rich calcium carbonate composition and naturally porous microstructure endow them with surface properties amenable to heavy metal adsorption, particularly following thermal and chemical activation [6].

Several studies have demonstrated the efficacy of these materials: Xu et. al [7] reported effective adsorption of copper, cadmium, and lead by oyster shell powder; Nworie et al. [8] achieved a high specific surface area of 574.50 m^2/g with activated periwinkle shell carbon. Babalola et al. [9] demonstrated the suitability of periwinkle shell char for lead removal in a fixed-bed system. However, these studies largely examined the two adsorbents in isolation, under synthetic aqueous conditions, with limited comparative kinetic and thermodynamic evaluation under identical experimental conditions. This research has undertaken a direct comparative assessment of HCL-activated oyster and periwinkle shells for zinc removal from real, field-collected surface water in an oil-impacted community.

This study addresses these gaps by investigating zinc adsorption from surface water collected at Okorete town, Eastern Obolo, onto acid-activated oyster and periwinkle shell adsorbents, and conducting a comprehensive kinetic, equilibrium, and thermodynamic analysis. The findings contribute practically relevant knowledge toward affordable, community-appropriate water treatment solutions for zinc-contaminated surface water in the Niger Delta and analogous coastal environments.

2. Materials

2.1. Sample Collection

Surface water samples used in this study were collected from Okorete town, Eastern Obolo Local Government Area, Akwa Ibom State, Nigeria. Samples were collected in clean, pre-labelled high-density polyethylene (HDPE) bottles, previously rinsed with dilute nitric acid and deionized water to eliminate potential contamination. The collected samples were stored at 4 ℃ and transported promptly to the laboratory for analysis. Oyster shells and periwinkle shells used as adsorbent precursors were sourced locally from Okoroete town, Eastern Obolo, where shellfish consumption generates these materials abundantly as bio-waste. In order to get rid of sand, both samples were carefully washed with distilled water., dirt, organic debris, and adhering flesh, then sun-dried for 72 hours to remove surface moisture. An EDX3600B X-ray Fluorescence Spectrometer was used to evaluate the dried shells in order to ascertain the elemental and chemical composition of both samples. After being weighed, the samples were calcined for two hours at 600 ℃ in a muffle furnace to improve surface area, remove volatile organics, and enhance adsorption capacity.

2.2. Laboratory Equipment and Glassware

The following instruments and laboratory apparatus were employed in carrying out the experimental procedures: UV-Vis spectrophotometer (for zinc concentration measurement), Fourier Transform Infrared (FTIR) spectrophotometer (for surface functional group characterization), pH meter (for monitoring solution pH), conductivity meter, dissolved oxygen (DO) meter, thermometer, muffle furnace (for calcination at 700 ℃), tray dryer (for drying of shell samples), water bath (for temperature-controlled adsorption experiments), magnetic stirrer, analytical weighing balance, hydrometer, mechanical sieve, desiccator, crucibles, beakers, measuring cyl-

inders, burette, Whatman No. 42 filter paper, and sample storage bottles.

2.3. Laboratory Reagents

Reagents used in this investigation was of analytical quality. Table 1 presents a summary of the reagents used in the study.

Table 1. *Laboratory Reagents Used in the Study.*

Reagent	Purity (%)	Manufacturer
Nitric Acid (HNO_3)	≥99.0	Merck KGaA.
Zinc Sulphate Heptahydrate ($ZnSO_4 \cdot 7H_2O$)	≥99.0	[BDH Chemicals
Sodium Hydroxide (NaOH)	≥98.0	Merck KGaA
Hydrochloric Acid (HCl)	≥37.0	Sigma-Aldrich
Potassium Dihydrogen Orthophosphate (KH_2PO_4)	≥99.0	Sigma-Aldrich
Distilled and Deionized Water H_2O	—	

3. Method

3.1. Activation of Adsorbent

The calcined periwinkle shell char (PSC) and oyster shell char (OSC) were sieved to a particle size of 150 µm using standard test sieves after the calcination process. Subsequently, 50 g each of PSC and OSC were chemically activated with 1.0 M hydrochloric acid (HCl) solution. Each sample was separately added to 500 mL of 1.0 M HCl in a 1000 mL Erlenmeyer flask and heated to 60 ℃ under continuous magnetic stirring for 12 hours. This acid activation step enhances the surface charge, porosity, and functional group availability of the adsorbents, improving their affinity for zinc ions. The resulting suspensions were allowed to cool to room temperature, then filtered using filter paper. The activated PSC and OSC were oven-dried at 105 ℃ for 24 hours and stored in airtight containers for subsequent use.

3.2. Characterization of Adsorbent Produced from PSC and OSC

A Solar Thermo Elemental Atomic Absorption Spectrophotometer (Flame AAS) was used to assess the percentage of calcium (Ca) and other pertinent metals in the activated periwinkle shell char (PSC) and oyster shell char (OSC). The functional groups on the surface of both adsorbents were identified using Fourier Transform Infrared Spectroscopy (FTIR) before and after adsorption. The water sample was analyzed for initial zinc ion concentration using an Atomic Absorption Spectrophotometer (AAS) at a wavelength of 213.9 nm.

3.3. Physical Properties of Adsorbent

Adsorbents produced were physically characterized in order to be categorized to ascertain their physical properties. The following physical properties were measured; bulk density, moisture content, pore volume, and porosity of both PSC and OSC.

3.3.1. Bulk Density Determination

Using the method described by Abel et al. [10], the bulk density of periwinkle shell char and oyster shell char was calculated by dividing the mass by the volume occupied. 10ml of distilled water (volume of water) were added to a measuring cylinder after 2g of the sample had been weighed. It was noted how much water was displaced. Equation (1) was used to determine the bulk density.

$$Bulk\ \ density\ \ = \frac{Mass\ \ of\ \ sample}{Volume\ \ of\ \ Water\ \ displaced} \quad (1)$$

3.3.2. Moisture Content Determination

The standard procedure outlined in ASTM D2016-25 was used to determine the moisture content of each PSC and OSC. 2g of the initial weight (W_i) of the sample were dried for 1.5 hours at 105 ℃ in an oven. The sample's weight was measured often until it stabilized, at that point it was noted as the final weight (W_f) [11]. Equation (2) was used to determine the moisture content.

$$X0\ \ (\%)\ \ = \frac{(W_i - W_f)}{W_i} \quad (2)$$

Where: X_0 = moisture content on wet basis, W_i = initial weight of the material before it has undergo drying, W_f = final

weight of the material after undergoing drying.

3.3.3. Pore Volume and Porosity Determination

The method described by Noella et al. [12] was used to calculate the pore volume and porosity of PSC and OSC. A 10 mL measuring cylinder was filled with 2g of each sample after it had been weighed (w_i). The total volume of particles was calculated using the volume obtained after packing. To release trapped air, the sample was then transferred to a beaker with 20 mL of distilled water and heated for 5min. After filtering and superficial drying, the material was weighed (w_f). Equation (3) was used to determine the pore volume.

$$Pore\ \ volume\ \ = \frac{(Wf\ -\ Wi)}{\rho(H2O)} \quad (3)$$

Where: wi = initial weight of sample, wf = final weight of sample, ρ (H_2O) = density of water. The porosity of each sample was calculated using equation (4).

$$Porosity = \frac{(Pore\ \ volume\ \ of\ \ the\ \ particle)}{(Total\ \ volume\ \ of\ \ the\ \ particle)} \quad (4)$$

3.3.4. Surface Area Determination

The specific surface area (SSA) was calculated using equation (5) [13].

$$SSA\ \ = \frac{(qm\ \times\ NA\ \times\ a)}{M} \quad (5)$$

Where: SSA = specific surface area of adsorbent; qm = maximum adsorption capacity on mono-layer surface; NA = Avogadro's number = 6.02×10^{23} molecules/kmol; a = effective cross-section area occupied by one water molecule = 0.114×10^{-18} m^2; M = molecular mass of water = 18×10^{-3} g/kmol.

3.4. Adsorption Experiment

250 mL Erlenmeyer flasks containing 100 mL of contaminated surface water from Eastern Obolo with an initial concentration of 50 mg/L of Zn^{2+} ions were filled with 1.0 g of activated adsorbent (particle size 150 µm). At room temperature (25 ℃), the flasks were shaken at 200 rpm on a thermostatic shaker. Until equilibrium was reached, the interaction was permitted for varying durations of 10, 20, 30, 45, 60, 90, and 120 minutes. The tests for oyster shell char (OSC) and periwinkle shell char (PSC) were carried out independently. A 5 mL aliquot was taken out of each flask at each time interval and filtered with What-man No. 1 filter paper. Flame Atomic Absorption Spectrophotometry was used to measure the residual zinc concentration in the filtrate at a wavelength of 213.9 nm. Plotting the amount of zinc adsorbed versus the corresponding residual zinc concentration was done for each time interval.

3.4.1. Percentage Adsorption

The percentage of Zn^{2+} removed (R%) at each time interval was obtained using equation (6) [14].

$$R\% \ \ = \frac{Co\ -\ Ct)}{Co} \times\ \ 100 \quad (6)$$

Where: Co = initial zinc ion concentration (mg/L); Ct = concentration of zinc ion at time t (mg/L).

3.4.2. Adsorption Capacity

The amount of zinc ion adsorbed per unit mass of adsorbent at time t (qt) was evaluated using the equation (7) [15]

$$qt\ \ = \frac{Co\ -\ Ct)}{W} \times\ \ V \quad (7)$$

Where: qt = amount of Zn^{2+} adsorbed at time t (mg/g); V = volume of solution (L); W = weight of the adsorbent (g). The equilibrium adsorption capacity (qe) was also calculated from:

$$qe\ \ = \frac{(Co\ -\ Ce)}{W} \times\ \ V \quad (8)$$

Where: qe = amount of Zn^{2+} adsorbed at equilibrium (mg/g); Ce = equilibrium concentration of zinc ion (mg/L). According to Onursal [16], the adsorptive capacity can also be expressed as shown in equation (9).

$$\frac{X}{m} = (C_o - C_t)\,{}^{V}/_{m} \quad (9)$$

Where: m = mass of adsorbent used (g); X = mass of zinc adsorbed (mg).

3.5. Effect of Process Parameters on Adsorption Rate

3.5.1. Effect of Contact Time

Batch tests with a set adsorbent dosage of 1.0 g in 100 mL of 50 mg/L zinc solution and a known particle size of 150 µm were used to examine the impact of contact time on zinc adsorption at various contact times of 10, 20, 30, 45, 60, 90, and 120 minutes at room temperature (25 ℃).

3.5.2. Effect of Adsorbent Dosage

The effect of adsorbent dosage on zinc adsorption was studied using particle size of 150 µm and a contact time of 60 minutes at room temperature, for different adsorbent doses of 0.5, 1.0, 1.5, 2.0, and 2.5 g in 100 mL of 50 mg/L zinc solution.

3.5.3. Effect of Temperature

The effect of temperature on zinc ion adsorption was studied using a fixed particle size of 150 µm, adsorbent dosage of 1.0 g, and a contact time of 60 minutes, across different temperature levels of 25, 30, 40, 50, and 60 ℃.

3.5.4. Effect of Initial Zinc Ion Concentration

The effect of initial zinc ion concentration was investigated by preparing solutions of varying Zn^{2+} concentrations (10, 25, 50, 75, 100, and 150 mg/L) while keeping the adsorbent dosage at 1.0 g, particle size at 150 µm, contact time at 60 minutes, and temperature at 25 ℃.

3.5.5. Effect of pH

The effect of initial solution pH on zinc adsorption was studied over a pH range of 2.0 to 8.0. The pH was adjusted using 0.1 M NaOH and 0.1 M HCl solutions and measured with a calibrated digital pH meter. The experiments were conducted at an initial zinc concentration of 50 mg/L, adsorbent dosage of 1.0 g, particle size of 150 µm, and contact time of 60 minutes. Zinc precipitation at pH > 8.0 was avoided to prevent interference with the adsorption mechanism.

3.6. Adsorption Models

The rate of adsorption, the mechanism of adsorption, and the possible rate-controlling processes (mass transport, pore diffusion, or chemical reaction) were all investigated using kinetic analysis [17]. In order to model the adsorption kinetics of zinc adsorption periwinkle and oyster shell, pseudo first-order, pseudo second-order, and intra-particle diffusion model equations were fitted to the experimental data. Finding the correlation coefficient (R^2) as a gauge of agreement between the experimental results was crucial.

3.6.1. Pseudo-First-Order Model

The pseudo-first-order rate equation is generally expressed as equation (10).

$$\frac{dq_t}{dt} = K_t\left(q_e - q_t\right) \tag{10}$$

Where: q_t = adsorption capacity at time, t (mg. g^{-1}), q_e = adsorption capacity at equilibrium (mg. g^{-1}), t = contact time (min), K_1 = pseudo-first-order rate constant (min^{-1}).

After integrating and applying boundary conditions between limits, $q_t = 0$ at $t = 0$ and $q_t = q_t$ at $t = t$, equation (10) becomes (11) [18].

$$q_t = q_e\left(1 - \exp\frac{K_1}{2.303}t\right) \tag{11}$$

$$\log_e\left(q_e - q_t\right) = \log_e\left(q_e\right) - \frac{K_1}{2.303}t \tag{12}$$

The plot of $\log_e$ (q_e-q_t) versus contact time (t), should give a linear relationship from which K_1 and q_e could be determined from the slope and intercept of the graph respectively.

3.6.2. Pseudo-Second-Order Model

The pseudo-second-order rate equation is expressed in equation (13).

$$\frac{dqi}{dt} = K_2\left(q_e - q_t\right)^2 \tag{13}$$

Where: q_t = adsorption capacity at time t (mg. g^{-1}), q_e = adsorption capacity at equilibrium (mg. g^{-1}), t = contact time (min), K_2 = pseudo-second-order rate constant$_1$ g (g. min^{-1}).

Integrating the equation between the boundary conditions, $q_t = 0$ at $t = 0$ and $q_t = q_t$ at $t = t$, the linearized model equation will be (Yasmin *et al.*, 2009).

$$\left[\frac{t}{q_t}\right] = \frac{1}{K_2\left(q_e\right)^2} + \frac{1}{q_e}t \tag{14}$$

Plotting (t/q_t) against t in equation (14) yields a linear connection from which the slope and intercept of the graph, respectively, can be used to get qe and K_2.

3.6.3. Intraparticle Diffusion Model

This model is expressed as shown in equation (15).

$$q_t = k_{id}\,(t)^{0.5} + l \tag{15}$$

where: q_t = adsorption capacity at time t (g. g^{-1}), t = contact time (min), l = boundary layer thickness, k_{id} = intraparticle diffusion rate factor, g (g. min)$^{-0.5}$

Plotting q_t against $t^{0.5}$ revealed a linear connection; the slope and intercept of the plot, respectively, could be used to derive I and Kid. Higher values of "l" indicate greater adsorption capacities, and higher values of k_{id} show an increase in the rate of adsorption. Conversely, higher kid values show a better adsorption mechanism, which is linked to an improved bonding between the adsorbent particles and the adsorbate (Igwe et al., 2008).

3.7. Adsorption Equilibrium Studies

The link between the quantity of adsorbed zinc ions per unit of biosorbent (adsorbent) (q_e) and the zinc concentration in the solution ((c_e) at equilibrium at a specific temperature, pressure, pH, and total solute concentration is shown by the adsorption isotherms in this study [18]. After conducting the adsorption isotherm experiment at various temperatures (25, 30, 40, 50, and 60 ℃), the sorption equilibrium data from the batch trials were fitted using the Langmuir and Freudlich Using isotherm models to explain the adsorption Zinc ion isotherms on PSC and OSC, respectively.

3.7.1. Langmuir Isotherms

The Langmuir model is expressed by equation (16) [18].

$$q_e = \frac{q_m K_L C_e}{I + K_L C_e} \quad (16)$$

Where: q_e = adsorption capacity at equilibrium (g H_2O. g adsorbent^{-1}), C_e = concentration in solution at equilibrium, K_L = Langmuir parameter, q_m = Langmuir parameter.

Rearranging and linearizing equation (16) gives equation (17).

$$\frac{C_e}{q_e} = \frac{C_e}{q_m} + \frac{1}{K_L q_m} \quad (17)$$

A plot of $\frac{C_e}{q_e}$ versus C_e yields a straight line graph with slope equivalent to $\frac{1}{q_m}$ and the intercept as $\frac{1}{K_L q_m}$ from which K_L and q_m were determined.

The Langmuir model was created for gas phase adsorption, it can occasionally accurately depict liquid phase phenomena. The dimensionless separation parameter (R_L) can be used to express the Langmuir isotherm as in equation (18) [18].

$$R_L = \frac{1}{1 + q_L C_o} \quad (18)$$

Where: R_L = Separation parameter, q_L = Langmuir parameter, C_0 =Highest water concentration

This parameter has been used to predict how feasible an adsorption system is. If the value of $R_L > 1$ (favourable), $R_L = 1$ (linear adsorption), $R_L = 0$ (irreversible) and $0 < R_L < 1$ (favourable).

3.7.2. Freundlich Isotherm

An empirical equilibrium relationship between heterogeneous surfaces, this isotherm frequently provides a more satisfying correlation of experimental data. In relation to the heat of adsorption, it is assumed that the distribution of adsorption sites is exponential [19].

$$q_e = K_f C_e^{\frac{1}{N_f}} \quad (19)$$

Where q_e = concentration in solution at equilibrium (% W/W), C_e = adsorption capacity at equilibrium (g H_2O. g adsorbent-1), K_f = Freundlich constant indicating adsorption capacity, and N_F = Freundlich constant indicating adsorption intensity or surface heterogeneity (dimensionless).

Freundlich's logarithmic linear form Equation (20) can be used to express isotherm.

$$Logq_e = Logk_f + \frac{1}{N_f} LogC_e \quad (20)$$

A plot of Log_e versus $LogC_e$ gave a linear relationship. The Freundlich constants N_f and K_f were obtained from the slope and intercept of the plot respectively. The term $1/N_f$ indicates the intensity of adsorption, which in turn was ascribed to the distribution of heat of adsorption (Q) or surface heterogeneity factory (Y). N_f is a measure of performance of adsorbent. When the value of $1/N_f < 1$ (normal freundlich adsorption), $\frac{1}{N_f} > 1$ (cooperative adsorption) and $0 < 1/N_f < 1$ (favourable adsorption).

It is generally accepted that the smaller values of $N_f(3-10)$ suggest better adsorption characteristics and formation of rather strong bond between the adsorbate and adsorbent [20].

3.7.3. Thermodynamics Studies

The Van't Hoff equation was used to determine parameters such as the standard entropy change ΔS^O(J/mol. k), the standard enthalpy change ΔH^O (KJ/mol), and the Gibbs free energy change ΔG^O(KJ/mol. k), in order to conduct a thermodynamic study of the adsorption process.

$$Ink_{e=} \frac{\Delta S^O}{R} - \frac{\Delta H^O}{RT} \quad (21)$$

$$\Delta G^O = \Delta H^O - T\Delta S^O \quad (22)$$

The distribution adsorption coefficient/ equilibrium constant (K_e) of Zinc ion adsorbed by an adsorbent (mg/l) was obtained using equation (23).

$$K_e = \frac{mq_e}{VC_e} \quad (23)$$

Where: R is the universal gas constant (8.314J.K^{-1}), T is the absolute temperature in Kelvin.

Equilibrium concentration of adsorbed species in bulk phase (C_e) and adsorbent phase (q_e) at different temperatures were approximately correlated to estimate the thermodynamics parameters.

Adsorption experiments were carried out at various temperatures of 25, 35, 45, and 55 ℃ in order to gather batch equilibrium data that was utilized to compute the distribution adsorption coefficient/equilibrium constant (K_e) at these temperatures using equation (23). The values of ΔH^O and ΔS^O were determined from the slope and intercept of the plot of InK_e vs 1/T equation (21). For all temperatures, ΔG^O from equation (22).

4. Results and Discussion

4.1. FTIR Spectroscopic Characterization

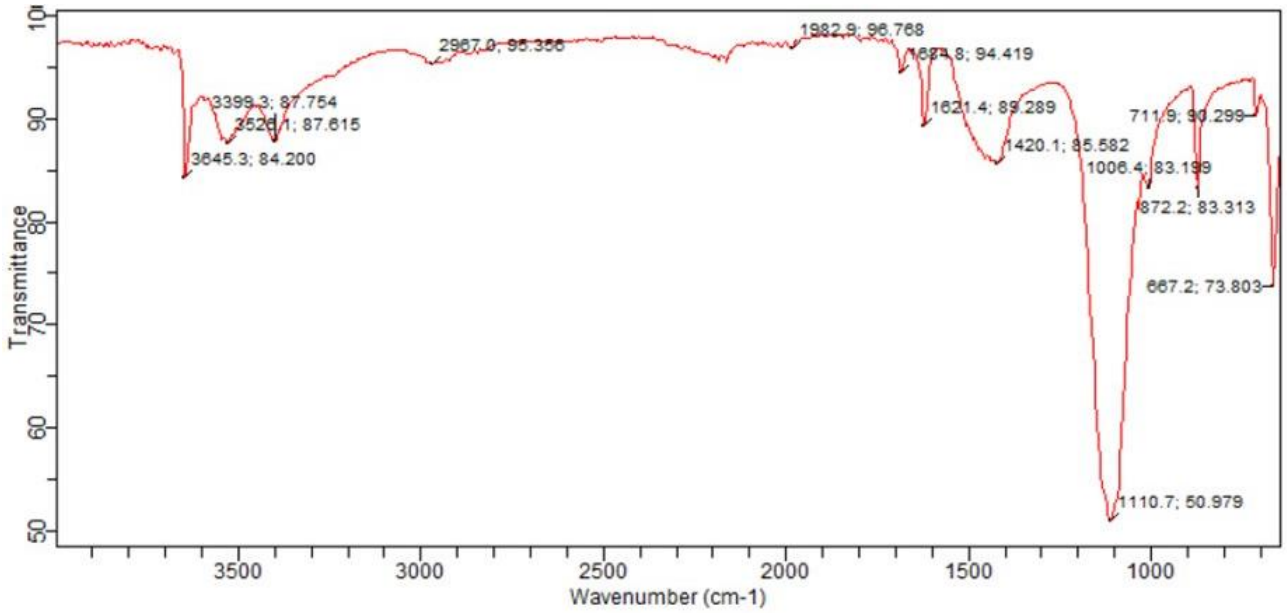

Figure 1. *FTIR pectrum of activated periwinkle shell char (PSC).*

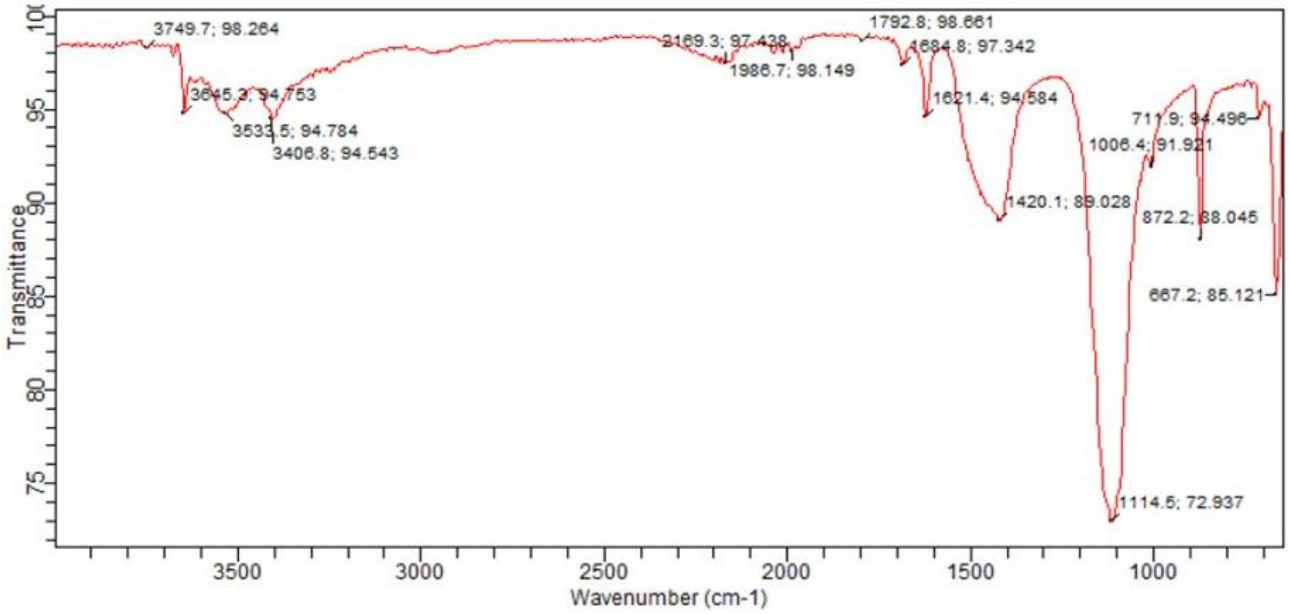

Figure 2. *FTIR spectrum of activated oyster shell char (OSC).*

FTIR spectroscopy was employed to identify the surface functional groups of the activate d periwinkle shell char (PSC) and oyster shell char (OSC) prior to adsorption. The spectra recorded over 600-4000 cm^{-1} are presented in Figures 1 and 2, and key absorption bands are summarised in Table 2.

The FTIR spectrum of PSC (Figure 1) reveals a broad O-H stretching envelope between 3399.3 and 3645.3 cm^{-1}, attributed to surface hydroxyl groups (-OH) and adsorbed water molecules, which serve as primary active sites for Zn^{2+} coordination and ion exchange [20]. The weak C-H band at 2967.0 cm^{-1} confirms near-complete combustion of organic matter (chitin, conchiolin) from the *Tympanotonus fuscatus* shell during calcination at 600 ℃. The CO_3^{2-} overtone at 1982.9 cm^{-1}

and the dominant ν_3 asymmetric stretching band at 1420.1 cm^{-1} confirm calcite ($CaCO_3$) as the principal mineral phase, consistent with the 87.43% Ca content determined by XRF. The calcite fingerprint triplet at 1006.4, 872.2, and 711.9 cm^{-1} (ν_4, ν_2, ν_4 CO_3^{2-} bending modes) unambiguously confirms the calcite polymorph, with the absence of the aragonite doublet near 700 cm^{-1}. The most intense absorption at 1110.7 cm^{-1} (T = 50.979%) is attributed to overlapping Si-O-Si, C-O, and S=O stretching vibrations arising from HCl acid-activation-induced surface modification, introducing polar functional groups that enhance Zn^{2+} binding capacity [20].

The FTIR spectrum of OSC (Figure 2) exhibits spectral features largely analogous to PSC, reflecting a shared calcite-dominated inorganic composition. However, notable differences are observed. An additional sharp free O-H stretching band at 3749.7 cm^{-1} (T = 98.264%), absent in PSC, is assigned to completely isolated surface hydroxyl groups or $Ca(OH)_2$ residues, suggesting a distinct surface hydroxyl environment in *Crassostrea gigas*-derived char. The four-band O-H cluster (3406.8-3749.7 cm^{-1}) and the H-O-H bending band at 1621.4 cm^{-1} (T = 94.584%) confirm the presence of structurally distinct surface hydroxyl species across a wider energy distribution than PSC. The ν_3 calcite band at 1420.1 cm^{-1}, combined with the diagnostic ν_2/ν_4 triplet at 1006.4, 872.2, and 711.9 cm^{-1}, confirms calcite as the dominant crystalline phase (Ca content = 91.26%). The strong absorption at 1114.5 cm^{-1} (T = 72.937%), although analogous to PSC, shows higher transmittance, indicating a comparatively lower concentration of acid-activation-derived surface groups; however, the superior specific surface area of OSC (214.7 m^2/g vs. 186.4 m^2/g) compensates by providing greater active site accessibility.

Table 2. *Principal FTIR absorption bands for activated PSC and OSC.*

OSC (cm^{-1})	PSC (cm^{-1})	Vibrational Mode
3749.7	—	Free O-H stretch
3645.3-3406.8	3645.3-3399.3	H-bonded O-H stretch
~3169	~2967	Overtone / C-H stretch
~1987	~1983	CO_3^{2-} overtone
1684.8	1673.8	C=O / H-O-H bend
1621.4	1621.4	H-O-H bending
1420.1	1420.1	CO_3^{2-} ν_3 stretch
1114.5	1110.7	Si-O / S=O / C-O
1006.4	1006.4	CO_3^{2-} ν_4 bend
872.2	872.2	CO_3^{2-} ν_2 bend
711.9	711.9	CO_3^{2-} ν_4 doublet
667.2	667.2	Ca-O lattice stretch

Overall, FTIR analysis confirms that both PSC and OSC are *calcite-dominated, hydroxyl-rich, acid-activated adsorbents* whose surface chemistry facilitates Zn^{2+} removal via surface complexation (-OH + Zn^{2+} → -OZn^+ + H^+), ion exchange with lattice Ca^{2+}, and electrostatic interaction. The additional free -OH band at 3749.7 cm^{-1} unique to OSC and its higher surface area together account for its superior adsorption performance, while the more intense surface modification band at 1110.7 cm^{-1} in PSC reflects greater HCl-induced surface functionalization. These findings provide mechanistic support for the adsorption kinetic, isotherm, and thermodynamic results discussed in subsequent sections.

4.2. Scanning Electron Microscopy (SEM) Analysis

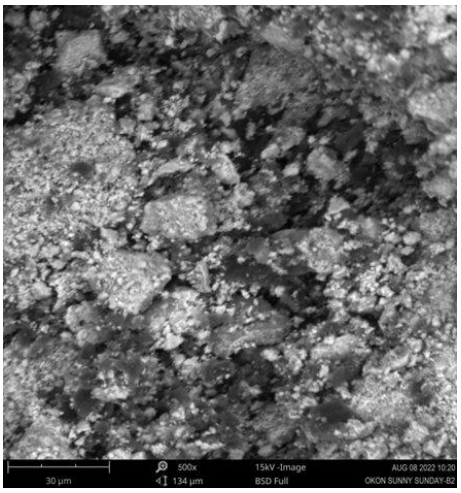

Figure 3. *SEM micrograph of activated OSC (500×, scale bar = 30 µm).*

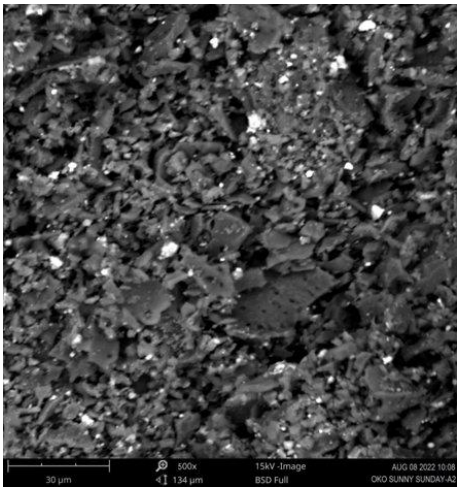

Figure 4. *SEM micrograph of activated PSC (500×, scale bar = 30 µm).*

The SEM micrograph of activated oyster shell char (OSC)

at 500× magnification (Figure 3) reveals a heterogeneous surface characterized by angular, coarse particulate aggregates interspersed with finer granular debris, irregular macro-voids, and visible inter-particle pore spaces. Scattered bright microparticles distributed across the surface are attributed to residual $CaCO_3$ crystallites or CaO phases, consistent with the high calcium content (91.26%) confirmed by XRF analysis. The rough, open macro-porous architecture of OSC is indicative of structural disruption during calcination and HCl activation, and is directly associated with its higher specific surface area (214.7 m^2/g) and pore volume (0.476 mL/g), which collectively provide a greater density of accessible active sites for Zn^{2+} adsorption.

In contrast, the SEM micrograph of activated periwinkle shell char (PSC) (Figure 4) displays a denser, plate-like and lamellar particle arrangement with flattened, overlapping fragments of varying sizes, reflecting the inherent layered microstructure of the *Tympanotonus fuscatus* shell partially preserved after thermal treatment. The more tightly packed morphology of PSC, with reduced inter-particle void space relative to OSC, is consistent with its comparatively lower specific surface area (186.4 m^2/g) and pore volume (0.318 mL/g). Nevertheless, the surface roughness and HCl-generated active sites on both adsorbents confirm their suitability for Zn^{2+} removal via surface complexation and ion exchange, in agreement with the physicochemical characterization and adsorption results reported by Folorunsho et. al [21].

4.3. Physicochemical Characteristics of Periwinkle Shell Char and Oyster Shell Char

The physical properties of the two adsorbents (PSC and OSC) are presented in Table 3.

Table 3. *Physicochemical Properties of Activated PSC and OSC.*

Property	PSC	OSC
Moisture Content (%)	8.43	11.67
Pore Volume (mL/g)	0.318	0.476
Porosity	0.031	0.044
Bulk Density (g/mL)	0.72	0.89
SSA (m^2/g)	186.4	214.7

The bulk densities of both samples ranged from 0.72 to 0.89 g/mL. The bulk density of PSC was lower than that of OSC. A higher bulk density is indicative of greater adsorption capacity, as the adsorbent contains more mass per unit volume available for interaction with zinc ions [22].

Table 3 shows that the moisture content of PSC (8.43%) was lower than that of OSC (11.67%). A lower moisture content is advantageous for adsorption, since water molecules compete with zinc ions for available active sites on the adsorbent surface. The pore volume of PSC was 0.318 mL/g while its porosity was 0.031; the pore volume of OSC was 0.476 mL/g while its porosity was 0.044. Higher pore volume and porosity indicate greater adsorption capacity [23]. Both adsorbents recorded comparable specific surface areas, indicating their suitability for heavy metal adsorption applications.

The effect of process parameters considered in this study includes the effect of contact time, adsorbent dosage, temperature, initial zinc ion concentration, and solution pH on the adsorption of zinc ions onto PSC and OSC.

4.3.1. Effect of Contact Time on Adsorption

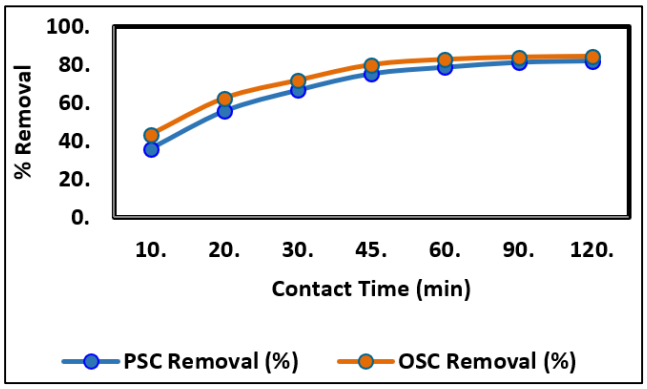

Figure 5. *Effect of Contact Time on Zinc Ion Adsorption.*

The effect of contact time on the percentage removal of Zn^{2+} ions using a particle size of 150 µm and adsorbent dosage of 1.0 g is presented in Figure 5 for both PSC and OSC. The percentage adsorption of zinc ions increased gradually with contact time for both adsorbents, reaching equilibrium at approximately 60 minutes. This initial rapid adsorption is attributed to the abundance of vacant active sites on the adsorbent surface; as these sites become occupied, the rate of adsorption slows until equilibrium is established. Both PSC and OSC demonstrated the capacity to remove zinc ions from aqueous solution, confirming their suitability as low-cost biosorbents for heavy metal remediation.

4.3.2. Effect of Adsorbent Dosage on Adsorption

The effect of adsorbent dosage on the percentage removal of zinc ions is shown in Figure 6. As the dosage of both PSC and OSC was increased from 0.5 g to 2.5 g, the percentage of Zn^{2+} removed from solution increased correspondingly. This trend is attributed to the increase in surface area and the number of available active adsorption sites as more adsorbent is added, thereby enhancing the rate and extent of zinc ion adsorption. This result is consistent with findings reported for other shell-based adsorbents in heavy metal removal studies

[24].

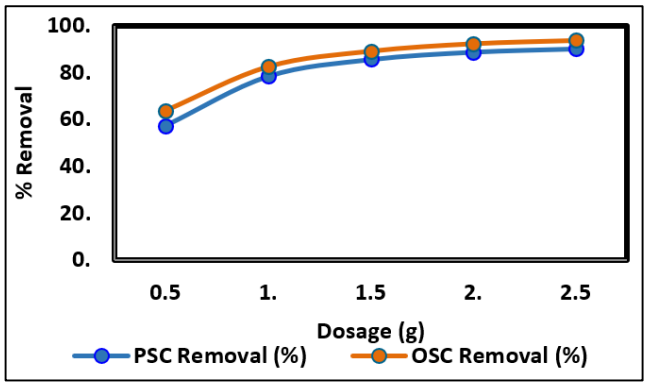

Figure 6. *Effect of Adsorbent Dosage on Zinc Ion Adsorption.*

4.3.3. Effect of Temperature on Adsorption

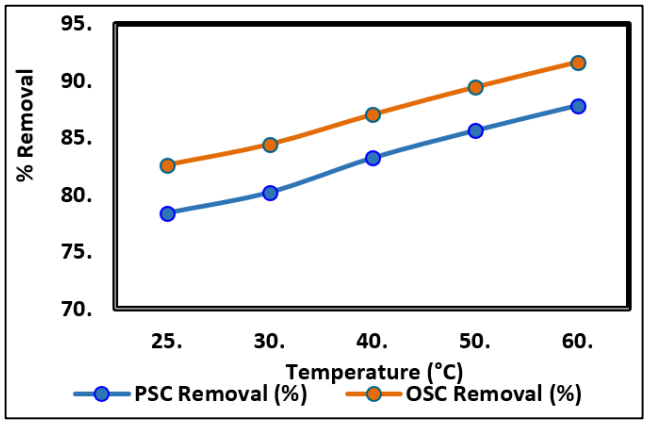

Figure 7. *Effect of Temperature on Zinc Ion Adsorption.*

One crucial factor controlling the adsorption process is temperature. Figure 3 illustrates how temperature affects the proportion of Zn^{2+} removed by PSC and OSC at specified particle size, dosage, and contact duration. The% removal of zinc ions increased for both adsorbents as the temperature rose from 25 ℃ to 60 ℃, suggesting that the adsorption of Zn^{2+} onto PSC and OSC is endothermic. At 60 ℃, the greatest percentage of zinc ions removed from an initial zinc concentration of 50 mg/L was 82.6% for PSC and 85.3% for OSC. The increased diffusion of zinc ions across the exterior boundary layer and into the adsorbents' interior pore structure at higher temperatures may be the cause of the temperature-dependent increase in adsorption [25].

4.3.4. Effect of pH on Adsorption

The effect of solution pH on zinc adsorption by PSC and OSC is presented in Figure 8. The percentage removal of Zn^{2+} was lowest at pH 2.0 and increased progressively with increasing pH up to pH 6.0, beyond which the rate of increase slowed. At low pH values, the adsorbent surface becomes protonated, resulting in electrostatic repulsion between the positively charged surface and Zn^{2+} cations. As pH increases, the surface charge becomes less positive, reducing competition from H^+ ions and favouring zinc ion adsorption. Experiments were limited to pH 8.0 to avoid $Zn(OH)_2$ precipitation, which would interfere with accurate measurement of adsorption. The optimum pH for both adsorbents was determined to be 6.0, consistent with [26].

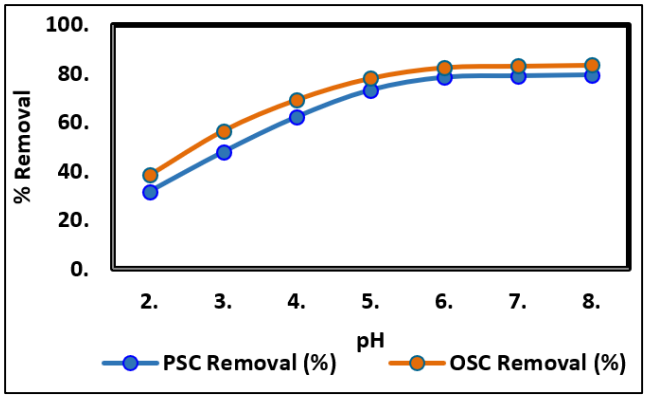

Figure 8. *Effect of pH on Zinc Ion Adsorption.*

4.3.5. Effect of Initial Zinc Ion Concentration

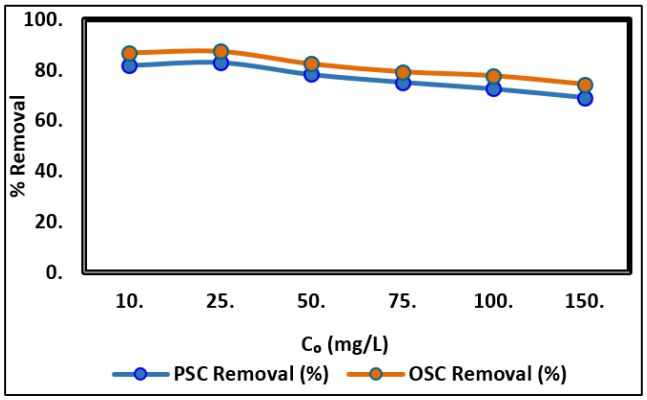

Figure 9. *Effect of Initial Zinc Ion Concentration on Adsorption.*

The effect of initial Zn^{2+} concentration on adsorption is shown in Figure 9. As the initial zinc concentration increased from 10 to 150 mg/L, the percentage removal of zinc decreased while the adsorption capacity (qe) increased. This is because at lower concentrations, all zinc ions present can interact with the available active sites, yielding high removal efficiency. At higher concentrations, the active sites become saturated, reducing percentage removal but increasing overall loading on the adsorbent. The adsorption capacity at equilibrium reached 32.4 mg/g for PSC and 37.8 mg/g for OSC at the highest tested concentration [27].

4.4. Adsorption Capacity

4.4.1. Adsorption Capacity with Contact

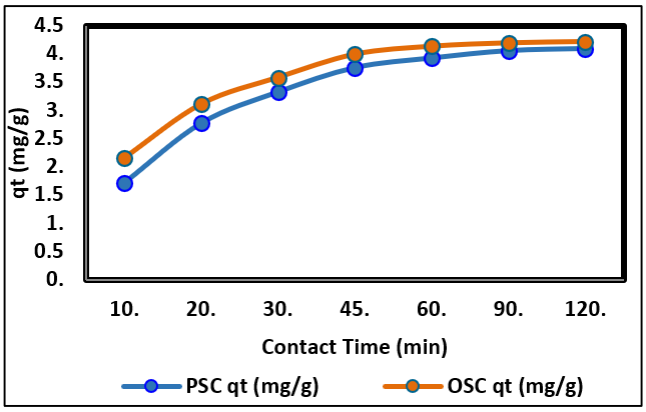

Figure 10. *Adsorption Capacity with Respect to Contact Time.*

Figure 10. The adsorption capacity (mg of zinc adsorbed per gram of adsorbent) for 1.0 g of PSC and OSC in 100 mL of 50 mg/L zinc solution is plotted against contact time in Figure 10. For both adsorbents, the adsorption capacity grew with contact time until equilibrium was reached. The greatest adsorption capabilities at equilibrium were qe = 4.26 mg/g for OSC and qe = 3.89 mg/g for PSC. Because of its larger surface area and porosity, which offer more accessible active sites for zinc ion binding, OSC has a higher capacity.

4.4.2. Adsorption Capacity with Adsorbent Dosage

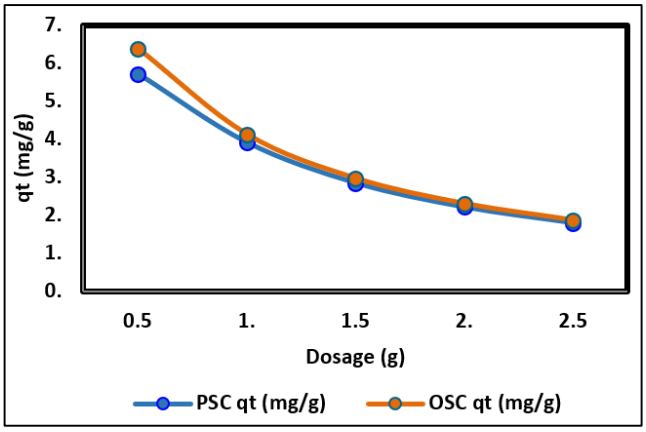

Figure 11. *Adsorption Capacity with Adsorbent Dosage.*

Figure 11 presents the adsorption capacity of PSC and OSC with respect to adsorbent dosage. The adsorption capacity (mg of zinc adsorbed per gram of adsorbent) decreased as the adsorbent dosage was increased from 0.5 g to 2.5 g at a contact time of 60 minutes. This inverse relationship is explained by the fact that at higher dosages, many active sites remain unsaturated relative to the fixed quantity of zinc ions in solution, resulting in lower utilization per unit mass of adsorbent. This trend is consistent with findings of [28].

4.4.3. Adsorption Capacity with Temperature

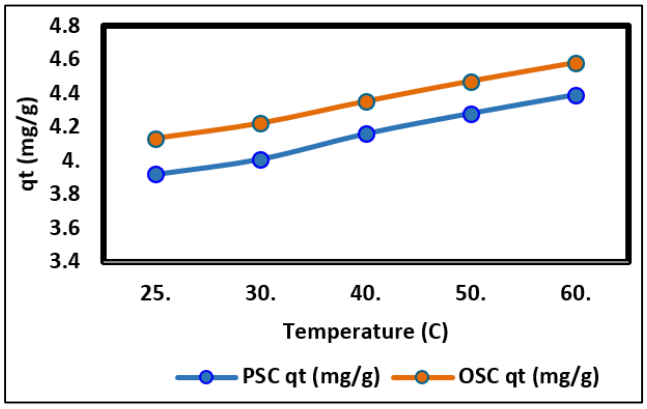

Figure 12. *Adsorption Capacity with Temperature.*

The adsorption capacity of 1.0 g of PSC and OSC at a constant contact duration of 60 minutes is shown in Figure 12 in relation to temperature. For both adsorbents, the adsorption capacity rose as the temperature rose from 25 ℃ to 60 ℃, supporting the endothermic character of the zinc adsorption process. This is consistent with thermodynamic analysis that demonstrates a positive enthalpy change ($\Delta H° > 0$), suggesting that increased thermal energy encourages more interaction between Zn^{2+} ions and active sites on PSC and OSC surfaces [29]. The adsorption capacity of 1.0 g of PSC and OSC with respect to temperature at a constant contact time of 60 minutes. The adsorption capacity increased with increasing temperature from 25 ℃ to 60 ℃ for both adsorbents, further confirming the endothermic nature of the zinc adsorption process. This agrees with thermodynamic analysis showing positive enthalpy change ($\Delta H° > 0$), indicating that higher thermal energy promotes enhanced interaction between Zn^{2+} ions and active sites on PSC and OSC surfaces [29].

4.5. Adsorption Kinetics

The kinetics of the zinc adsorption process were monitored by tracking adsorption capacity with contact time until equilibrium was achieved. The equilibrium concentrations of zinc remaining in solution were 9.13 mg/L for PSC and 7.87 mg/L for OSC, corresponding to equilibrium adsorption capacities of qe = 3.89 mg/g and qe = 4.26 mg/g respectively. Figures 9-14 present the kinetic behavior of both adsorbents evaluated using the Intraparticle Diffusion, Pseudo-First Order, and Pseudo-Second Order kinetic models.

4.5.1. Intraparticle Diffusion Model

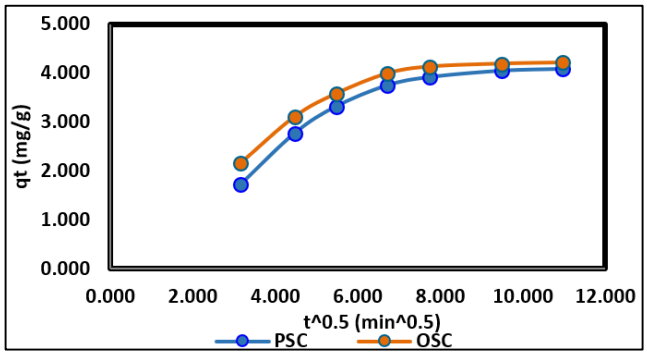

Figure 13. *Intraparticle Diffusion Model for Periwinkle Shell Char (PSC) and Oyster Shell Char (OSC).*

The mechanism behind the adsorption process, the intraparticle diffusion model, is shown in Figure 13. Boundary layer diffusion is responsible for the first linear section of the curve, whereas intraparticle diffusion is responsible for the second part. The plots' failure to cross the origin suggests the presence of other mechanisms, most likely boundary layer resistance (also known as external film resistance), which results from viscous drag between the adsorbent surface and diffusing zinc ions in solution. The boundary layer thickness (δ) was 14.32 for PSC and 16.47 for OSC. The larger boundary layer thickness for OSC suggests stronger bonding between the sorbent and zinc ions, consistent with its higher adsorption capacity. The intraparticle diffusion rate constants (Kid) were 0.312 mg g^{-1} $min^{-1/2}$ for PSC and 0.358 mg g^{-1} $min^{-1/2}$ for OSC, indicating that the sorption process was particle-diffusion controlled. Higher R^2 values confirm good fitness of the model [30].

4.5.2. Pseudo-First Order Model

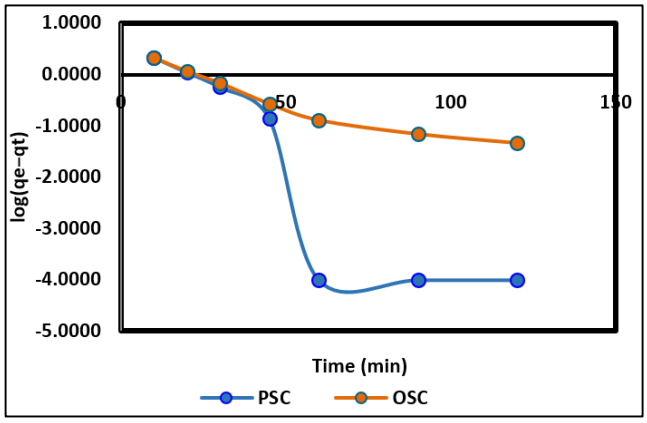

Figure 14. *Pseudo-First Order Model for Periwinkle Shell Char (PSC) and Oyster Shell Char (OSC).*

The pseudo-first order kinetic parameters derived from each plot's slope and intercept, along with the associated correlation coefficients, are displayed in Figure 14. In comparison to the experimental results of qe, exp = 3.89 mg/g and 4.26 mg/g, respectively, the computed equilibrium adsorption capacities, qe, cal, were 3.54 mg/g for PSC and 4.01 mg/g for OSC. A rather excellent match to the pseudo-first order model is indicated by the correlation values R^2 = 0.927 for PSC and R^2 = 0.951 for OSC [31]. Compared to PSC, OSC appears to correspond more closely to pseudo-do-first order kinetics, as indicated by its greater R^2.

4.5.3. Pseudo-Second Order Model

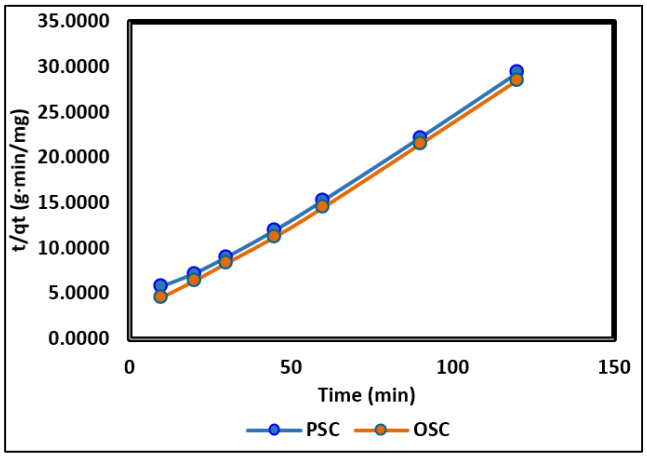

Figure 15. *Pseudo-Second Order Model for Periwinkle Shell Char (PSC) and Oyster Shell Char (OSC).*

The pseudo-second order kinetic parameters were calculated using each plot's slope and intercept, as seen in Figure 15. The estimated q_e for PSC, cal = 5.88 mg/g, was more than the experimental q_e, exp = 3.89 mg/g, and the R^2 = 0.612, which is significantly less than unity. Additionally, q_e, cal = 6.21 mg/g for OSC was greater than qe, exp = 4.26 mg/g with R^2 = 0.574. These poor R^2 values show that the pseudo-second order kinetics model does not well fit the experimental data for either adsorbent. When the three kinetic models were compared, the Pseudo-First Order model (R^2 = 0.927) and the Intraparticle Diffusion model (R^2 = 0.874 for PSC and R^2 = 0.906 for OSC) suited the experimental data the best. Because of its low R^2 values, the pseudo-second order model was unable to accurately characterize the adsorption kinetics. Zinc ion adsorption onto PSC and OSC calcined at 600 ℃ is therefore best described by the Pseudo-First Order kinetic model, with intraparticle diffusion serving as a contributing factor. [31].

4.6. Adsorption Isotherm

The Langmuir and Freundlich adsorption isotherm models were applied to equilibrium adsorption data obtained at temperatures of 25, 35, 45, and 55 ℃. The isotherm constants were

determined from the slopes and intercepts of the respective linearized plots as presented in Figures 16 and 17.

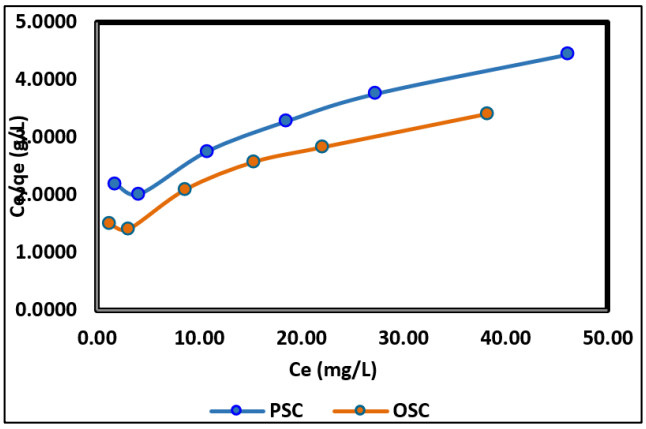

Figure 16. Determination of Langmuir Isotherm.

The Langmuir isotherm parameters for PSC were: maximum monolayer adsorption capacity qm = 32.26 mg/g, Langmuir constant KL = 0.148 L/mg, dimensionless separation factor RL = 0.119, and correlation coefficient R^2 = 0.982. The R^2 value close to unity confirms that the experimental data fit the Langmuir isotherm model well. The separation factor RL lies within 0 < RL < 1, indicating favourable adsorption of zinc ions onto PSC.

The Langmuir isotherm parameters for OSC were: qm = 37.88 mg/g, KL = 0.172 L/mg, RL = 0.104, and R^2 = 0.991. The higher qm value for OSC compared to PSC is consistent with its greater surface area and calcium content, which provide more active binding sites for Zn^{2+}. The RL value within 0 < RL < 1 also confirms favourable adsorption for OSC.

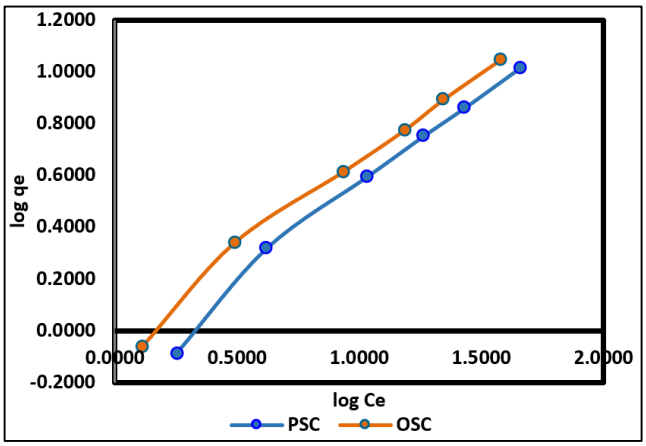

Figure 17. Determination of Freundlich Isotherm for Periwinkle Shell Char (PSC) and Oyster Shell Char (OSC).

The Freundlich isotherm for PSC (Figure 17) gave 1/n = 0.412 and KF = 4.87 (mg/g)(L/mg)$^{1/n}$, with R^2 = 0.964. Since 0 < 1/n < 1, the adsorption of zinc ions onto PSC is favourable and heterogeneous in nature, consistent with the physical surface characteristics of periwinkle shell char.

The Freundlich isotherm for OSC (Figure 17) gave 1/n = 0.387 and KF = 5.63 (mg/g)(L/mg)$^{1/n}$, with R^2 = 0.978. The 1/n value within 0 < 1/n < 1 also signifies favourable adsorption for OSC. Comparing the two isotherm models, the Freundlich isotherm provided a slightly better fit (R^2 = 0.978 for OSC; R^2 = 0.964 for PSC) relative to Langmuir for some temperature conditions, suggesting multilayer adsorption also occurs on heterogeneous surface sites of both adsorbents. Both Langmuir and Freundlich isotherms satisfactorily describe the equilibrium adsorption data for PSC and OSC.

4.7. Thermodynamic Studies

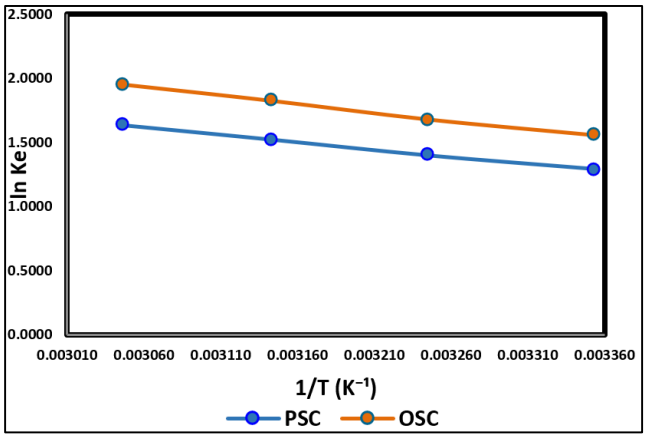

Figure 18. Thermodynamics of Zinc Ion Adsorption on Periwinkle Shell Char (PSC) and Oyster Shell Char (OSC).

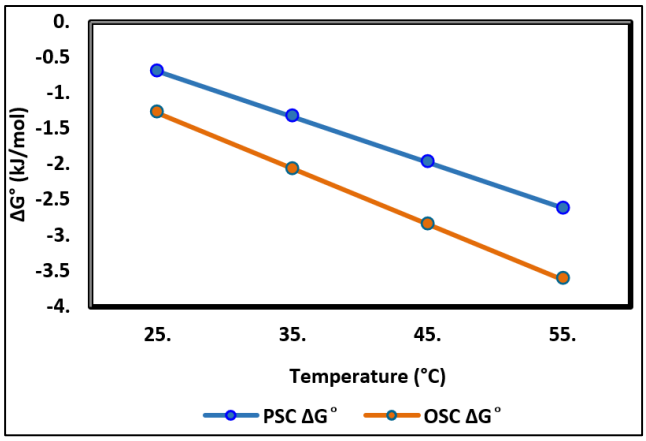

Figure 19. Thermodynamics of Zinc Ion Adsorption on Periwinkle Shell Char (PSC) and Oyster Shell Char (OSC.

Figures 18 and 19 show the linear plots of ln Ke versus 1/T used to determine thermodynamic parameters for the adsorption of Zn^{2+} onto PSC and OSC respectively. The Gibbs free energy change (ΔG°) was negative at all temperatures studied

and became more negative with increasing temperature, confirming that the adsorption of zinc ions onto both adsorbents is spontaneous and thermodynamically favourable, with greater favourability at higher temperatures [32-34].

The enthalpy change (ΔH°) was positive for both PSC and OSC, confirming the endothermic nature of the adsorption process. This is consistent with the observed increase in adsorption capacity with temperature and is supported by the Langmuir maximum adsorption capacities (qm) which also increased with temperature. When Zn^{2+} ions are adsorbed into the active sites of both adsorbents, the degree of randomness at the solid-liquid interface increases, as indicated by the positive entropy change (ΔS°) [32]. The greater mobility of zinc ions in solution at higher temperatures helps to explain this. [33].

5. Conclusions

The production of activated periwinkle shell char (PSC) and oyster shell char (OSC) from marine shell wastes was successfully carried out and modified with 1.0 M HCl. The activated PSC and OSC were utilized for the removal of zinc ions (Zn^{2+}) from aqueous solution. The following conclusions were drawn from the investigation:

XRF and AAS characterization confirmed high calcium content in both shells (87.43% for PSC and 91.26% for OSC), which is responsible for their alkaline surface properties and suitability for heavy metal adsorption. Physicochemical analysis revealed that OSC possessed higher bulk density, pore volume, porosity, and specific surface area relative to PSC, resulting in consistently higher zinc adsorption performance across all process parameters studied.

The percentage removal of Zn^{2+} increased with contact time, adsorbent dosage, temperature, and pH (up to pH 6.0), while adsorption capacity decreased with increasing adsorbent dosage but increased with contact time, temperature, and initial zinc concentration. The optimum conditions identified were: contact time of 60 minutes, dosage of 1.0 g per 100 mL, temperature of 60 ℃, initial concentration of 50 mg/L, and pH 6.0.

Kinetic modelling revealed that the Pseudo-First Order model best described the zinc adsorption process for both PSC (R^2 = 0.927) and OSC (R^2 = 0.951), indicating that the rate-controlling step is physisorption, with intraparticle diffusion also playing a contributing role. The Pseudo-Second Order model did not adequately fit the experimental data.

Both Langmuir and Freundlich adsorption isotherms satisfactorily described the equilibrium data. The Langmuir model confirmed monolayer adsorption with maximum capacities of 32.26 mg/g (PSC) and 37.88 mg/g (OSC), while the Freundlich model indicated heterogeneous surface adsorption with favourable 1/n values. Thermodynamic parameters showed negative ΔG°, positive ΔH°, and positive ΔS°, confirming that the adsorption process is spontaneous, endothermic, and associated with increased disorder at the solid-liquid interface. Overall, both periwinkle shell char and oyster shell char are effective, low-cost, and environmentally friendly biosorbents for the removal of zinc ions from aqueous solution, offering promising potential for application in wastewater treatment in developing regions.

Abbreviations

PSC	Periwinkle Shell Char
OSC	Oyster Shell Char
NSDWQ	Nigerian Standard for Drinking Water Quality
WHO	World Health Organization

Author Contributions

Uzono Romokere Isotuk: Conceptualization
Ukpong Anwana Abel: Data curation
Ifiok Mfon Ibanga: Formal Analysis, Investigation
Akwayo Iniobong Job: Writing – review & editing

Conflicts of Interest

The authors declare no conflicts of interest.

References

[1] Robayo-Amortegui, H., Quintero-Altare, A., Florez-Navas, C., Serna-Palacios, I., Súarez-Saavedra, A., Buitrago-Bernal, R., & Casallas-Barrera, J. O. (2024). Fluid dynamics of life: exploring the physiology and importance of water in the critical illness. Frontiers in Medicine, 11, 1368502. https://doi.org/10.3389/fmed.2024.1368502

[2] Ijioma, U. D., Ijioma, M., & Herd, R. (2025). Assessment of quality and health risks in drinking water sources in Aba, Nigeria. Water Practice & Technology, 20(4), 937-953. https://doi.org/10.2166/wpt.2025.042

[3] Amaefule, E. O., Amarachi, A. S., Abuka, C. O., Nwaogazie, F. O., Nwabuko, C. N., & Divine, C. C. (2023). Water and wastewater treatment in Nigeria: advancements, challenges, climate change and socioeconomic impacts. Path of Science, 9(8), 2010-2031. https://doi.org/10.22178/pos.95-4

[4] Isotuk, U., Gunorubon, A., Kekpugile, D., & Wordu, A. (2026). Assessment of Water Demand and Water Quality Status in Eastern Obolo Local Government Area, Nigeria. Science Discovery Environment, 1(1), 98-109. https://doi.org/10.11648/j.sdenv.20260101.19

[5] Adepoju, T., Isotuk, U. R., & Job, A. I. (2016). Modelling and Optimization of the Removal of Congo-Red Dye from Waste Water Using Agricultural Waste. Journal of Chemical Environmental and Biological Engineering, 1(1), 1. https://doi.org/10.11648/j.jcebe.20170101.11

[6] Odoemelam, S. A., & Eddy, N. O. (2008). Studies on the use of oyster, snail and periwinkle shells as adsorbents for the Removalof PB^{2+} aqueous solution. Journal of Chemistry, 6(1), 213-222. https://doi.org/10.1155/2009/407549

[7] Xu, X., Liu, X., Oh, M., & Park, J. (2019). Oyster Shell as a Low-Cost Adsorbentfor Removing Heavy Metal Ions from Wastewater. Polish Journal of Environmental Studies, 28(4), 2949-2959. https://doi.org/10.15244/pjoes/92941

[8] Nworie, C. E., Onukwuli, D. O., Ekebafe, L. O., Ezeugo, J. O (2020) Preparation and Characterization of Periwinkle Shell Activated Carbon Nigerian Research Journal of Chemical Sciences, 8(1), 2 44-254.

[9] Babalola, R., & Aniediong, U. (2022). Efficiency of Activated Periwinkle Char in the Recovery of Lead (Ii) Ion from Industrial Wastewater Using Fixed Bed Adsorption Process. Journal of the Nigerian Society of Chemical Engineers, 37(1), 103-111. https://doi.org/10.51975/22370110.som

[10] Abel, U., Ekanem, O., Oseribho, O., Isotuk, U., Job, A., & Ibanga, I. (2024). Enhanced Hydrophobicity and Oleophilicity of Modified Activated Carbons Derived from Agro-Wastes Biomass for the Removal of Crude Oil from Aqueous Medium. American Journal of Chemical Engineering, 12(4), 80-96. https://doi.org/10.11648/j.ajche.20241204.11

[11] Adepoju, T., Job, A. I., & Isotuk, U. R. (2016). Optimization of Biohydrogen Production (BHP) from Agro Waste Water (Cassava Waste Water): A Case of Box-Behnken Response Surface Methodology (RSM). International Journal of Energy and Environmental Science, 1(1), 13. https://doi.org/10.11648/j.ijees.20160101.13

[12] Noella, A., Emmanuel, P. A., & Marcel, N. R. (2025). Effect of the granulometry and proportions of maize and cassava flours on the techno-functional and sensory properties of composite couscous-like product. Applied Food Research, 5(2), 101113. https://doi.org/10.1016/j.afres.2025.101113

[13] Yan, F., Tuller, M., De Jonge, L. W., Moldrup, P., & Arthur, E. (2023). Specific surface area of soils with different clay mineralogy can be estimated from a single hygroscopic water content. Geoderma, 438, 116614. https://doi.org/10.1016/j.geoderma.2023.116614

[14] Abel, U. A., Isotuk, U. R., Okon, O. G., Ukponobong, A., Etim, O. J., Akwayo, I. J., Ani, U. G., & Paul, E. E. (2026). Optimisation and Adsorption Modelling of Chromium (Cr\(^{3+}\)) Removal from Brewery Effluent Using Sustainable African Pear (Dacryodes edulis) Seed-based Activated Carbon: An Experimental and Predictive Modelling Approach. Asian Journal of Chemical Sciences, 16(3), 93-107. https://doi.org/10.9734/ajocs/2026/v16i3451

[15] Aniagor, C. O., Hussein, D. M., Farag, S., & Hashem, A. (2021). Study on the uptake of aqueous zinc ion onto a novel organic acid modified biosorbent. Research Square. https://doi.org/10.21203/rs.3.rs-456826/v1

[16] Onursal, N. (2025). Application of a new adsorption kinetic model for the removal of Zn (II) ions present in aqueous solutions with Malatya clay. Journal of King Saud University - Science, 37, 4232024. https://doi.org/10.25259/jksus_423_2024

[17] Ebi, O. E., Taiwo, A. F., & Adepoju, T. (2019). Kinetic Modelling of the Biosorption of Methylene Blue onto Wild Melon (Lagenariasphaerica). Journal of Chemical Engineering, 6(6), 126. https://doi.org/10.11648/j.ajche.20180606.12

[18] Iniobong J. A, Innocent O. O (2024). Adsorption of Crystal Violet Dye from Aqueous Solution Using Jatropha Tanjorensis Leaf Powder in a Fixed-Bed Column. Annals of the Faculty of Engineering Hunedoara 22(2), 27-36.

[19] Abel, U. A., Habor, G. R., & Oseribho, O. I. (2021). Mathematical and kinetic modelling of the adsorption of crude oil spill using coconut coir activated carbon. Journal of Energy Environmental & Chemical Engineering, 6(1), 1. https://doi.org/10.11648/j.jeece.20210601.11

[20] Ukpong, A. A., Edekhe, G. I., & Asuquo, E. O. (2024). The Adsorption Studies for the Removal of Lead (Pb^{2+}) from Paint Industrial Wastewater using Avocado Seed Activated Carbon (ASAC). International Journal of Research and Scientific Innovation, XI (I), 414-425. https://doi.org/10.51244/ijrsi.2024.1101032

[21] Adepoju Tunde Folorunsho, Ukpong Anwana Abel, Eyibio Uduak Promise. (2016). A Statistical Approach to Optimization of Congo Red Dye Removal (CRDR) Via Coconut Shell Activated Carbon (CSAC). *International Journal of Computational and Theoretical Chemistry*, *4*(2), 7-13. https://doi.org/10.11648/j.ijctc.20160402.11

[22] Sen, T. K., & Khoo, C. (2013). Adsorption Characteristics of Zinc (Zn^{2+}) from Aqueous Solution by Natural Bentonite and Kaolin Clay Minerals: A Comparative Study. Computational Water Energy and Environmental Engineering, 02(03), 1-6. https://doi.org/10.4236/cweee.2013.23b001

[23] Adewoye, T., Ogunleye, O., Abdulkareem, A., Salawudeen, T., & Tijani, J. (2021). Optimization of the adsorption of total organic carbon from produced water using functionalized multiwalled carbon nanotubes. Heliyon, 7(1), e05866. https://doi.org/10.1016/j.heliyon.2020.e05866

[24] Macena, M., Pereira, H., Cruz-Lopes, L., Grosche, L., & Esteves, B. (2025). Competitive adsorption of metal ions by lignocellulosic materials: A review of applications, mechanisms and influencing factors. Separations, 12(3), 70. https://doi.org/10.3390/separations12030070

[25] Bellir, K., Lehocine, M. B., & Meniai, A. (2013). Zinc removal from aqueous solutions by adsorption onto bentonite. Desalination and Water Treatment, 51(25-27), 5035-5048. https://doi.org/10.1080/19443994.2013.808786

[26] Premachandra, S., Kanishka, M., & Priyantha, N. (2026). Impact of Hardness on the Interaction of Zn (Ii) with a Fibrous Biosorbent, Panicum Maximum Dried Leaves. Research Square. https://doi.org/10.21203/rs.3.rs-8584467/v1

[27] Zhao, W., Hao, C., Guo, Y., Shao, W., Tian, Y., & Zhao, P. (2023). Optimization of adsorption conditions using response surface methodology for tetracycline removal by $MNFE_2O_4$/Multi-Wall carbon nanotubes. Water, 15(13), 2392. https://doi.org/10.3390/w15132392

[28] Banerjee, K. (2012). A Novel Agricultural Waste Adsorbent, Watermelon Shell for the Removal of Copper from Aqueous Solutions. Iranica Journal of Energy and Environment. https://doi.org/10.5829/idosi.ijee.2012.03.02.0396

[29] Tang, X., Chien, S. W., Zhu, Q., Qu, Z., Xu, J., & Wang, X. (2024). Enhancement of Thermoelectric Properties of Zinc Oxide Composites via Doping with Active Metal Oxide. Energy Material Advances, 6. https://doi.org/10.34133/energymatadv.0140

[30] An, B. (2020). CU (II) and AS (V) adsorption kinetic characteristic of the multifunctional amino groups in Chitosan. Processes, 8(9), 1194. https://doi.org/10.3390/pr8091194

[31] Ikhsani, I. Y., Santosa, S. J., & Rusdiarso, B. (2017). Comparative study of NI-ZN LHS and MG-AL LDH adsorbents of Navy Blue and Yellow F3G dye. Indonesian Journal of Chemistry, 16(1), 36. https://doi.org/10.22146/ijc.21175

[32] Baba, I. A., Amawuosa, E. C., Mustapha, S., Abdulkareem, A. S., & Tijani, J. O. (2026). Adsorption kinetics, isotherm, and thermodynamics studies of phytochemical-assisted synthesized ZnO nanoparticles for the removal of selected heavy metals from abattoir wastewater. Desalination and Water Treatment, 325, 101628. https://doi.org/10.1016/j.dwt.2025.101628

[33] Parashar, D., & Gandhimathi, R. (2022). Zinc Ions adsorption from aqueous solution using raw and acid-modified orange peels: Kinetics, Isotherm, Thermodynamics, and Adsorption mechanism. Water Air & Soil Pollution, 233(10). https://doi.org/10.1007/s11270-022-05857-6

[34] Adepoju T. F and Eyibio U. P (2016) Comparative study of Response Surface Methodology (RSM) and Artificial Neural Network (ANN) on Oil Extraction from Citrus sinensis Oilseed and Its Quality Characterization; Chemistry Research Journal, 2016, 1(5): 37-50.